energies

MDPI

Article

Practical Application Study for Precision Improvement Plan for Energy Storage Devices Based on Iterative Methods

Jaewan Suh [1], Minhan Yoon [2,*] and Seungmin Jung [3,*]

[1] Department of Electrical Engineering, Dongyang Mirae University, Seoul 08221, Korea; jwsuh@dongyang.ac.kr
[2] Department of Electrical Engineering, Kwangwoon University, Seoul 01897, Korea
[3] Department of Electrical Engineering, Hanbat National University, Daejeon 305-719, Korea
* Correspondence: minhan.yoon@gmail.com (M.Y.); seungminj@hanbat.ac.kr (S.J.); Tel.: +82-42-821-1096 (S.J.)

Received: 29 December 2019; Accepted: 1 February 2020; Published: 4 February 2020

Abstract: In the aspect of power grid, attention is being given to conditions of environmental variation along with the need for precise prediction strategies based on control elements in recently designed large-scale distributed generation systems. With respect to distributed generators, an operational prediction system is used to respond to the negative impacts that could be generated. As an active response plan, efforts are being made by system operators to cover fluctuations with utilization of battery-based storage devices. Solar or ocean energy that shares electrical structure with an energy storage system has recently being seen as a combined solution. Although this structure is supported by a state analysis plan, such methods must be performed within the range where the response is possible under consideration of the power requirements of the electronic devices. This paper focuses on an iterative based solution for enhancing response of storage that included in DC generation system, to check its availability in terms of possible calculation load. A previous storage management plan was utilized and tested using a commercially available transient electromagnetic simulation tool that focused on possible delays. Case studies were performed sequentially on the time delays based on utilizable inverter topologies.

Keywords: PV diagnosis; ESS application; DC power flow; calculation load; iterative methods

1. Introduction

Recent advances in the field of energy has shown that the penetration rate of photovoltaic (PV) power generation is expected to increase steadily over the next decade [1]. The existing small-scale PV systems dominating local demand has been replaced with bulk farm systems to take advantage of environmentally friendly policies as described in [2]. Until now, network operators have focused on the characteristics of large-scale power generation systems and have focused on increasing its capacity. To add to this, the demand for properly managed generated power has been derived due to grid expansion. The recently revised IEEE-1547, particular momentary cessation, illustrates these requirements of related industrial sectors [3]. Currently, PV systems with a capacity of one gigawatt or more are implemented worldwide, including an operating system to enable compliance with directives of system operators. In a PV farm, several sets of megawatt (MW) arrays are built, which should interact with centralized topologies. The need for a control strategy that focuses on the detailed specification of PV is increasing and may be a major challenge in the power system industry that focuses on stochastic uncertainty.

Although renewable energies supply smoothed energy by composing a farm network, the operators still demand advanced solutions for flexible power management with additional compensators [4,5].

However, most major storage applications are still geared to play a role in responding to demand rather than providing real-time compensation [6]. As described in [7], since the requirements in terms of response between the farm and operators have expanded, the power system industry has considered advanced real-time solutions. The study in [8], depending on the various practical conditions, emphasizes the importance of real/reactive compensation response. Reactive power compensation generally focuses on voltage fluctuations in the local energy system, but conversely, real power compensation requires control that focuses on supply and demand of the entire system. These real power reactions are achieved with the aid of detailed backup control of the energy storage system (ESS) based on power conversion systems (PCSs) which are performed with optimized signals generated according to the main system criteria as in [9–11].

Newly developed renewable energy has been generalized to connect to a grid through full-converter based PCS. A process for combining renewable sources has been commercialized with a study on how to treat an independent DC section as a cluster as in the concept of multi-terminal DC [12]. The main objective of this approach is to improve its control capability by sharing the imposed order from a transmission system operator (TSO) with each distributed energy source (DES) in the cluster. Since PV requires a relatively small geographical area, the concept has been preferentially applied to existing farms along with possible storage system [11]. In a PV based hybrid DC system, which adopts a storage application, to perform precise control in a region where there is a number of DESs, a compensatory calculation process for each signal may be necessary. With regards to this, a proposal about a voltage calculation method based on a power flow analysis that considers the current flow between the PV modules is presented in [13], with detailed description of a practical ESS application. The possible voltage fluctuations generated between cables which were reported in [14,15] was reflected and analyzed in [13].

In this paper, in the signal dispatch process of a hybrid system, a feasibility analysis about proceeding with order management while calculating an appropriate voltage was derived. The main objective was to check the feasibility of an ESS compensation scheme which applies a voltage signal calibration in order to implement a power management plan for a hybrid system according to the applied load. Previous formula descriptions were expanded to enable it to deal with practical voltage variations. To carry out a practical approach in which an included PCS controller manages not only the voltage of each DC section but also the calculation delays, a simulation analysis was studied and confirmed with the consideration of real power that changes continuously. Focusing on a distribution network, the voltage impact was established and analyzed to check the availability of additional signal compensation plan. The ESS model configurations, including control topologies, are composed as in [13] to implement a reasonable case design.

2. Electrical Components

2.1. General Objective

The power flow calculation is a conventional method used in the power system analysis to confirm not only the power supply condition but also the status of each bus [16]. In general, it is based on the Newton–Raphson method of AC power system analysis without the consideration of grid scale as investigated in some literatures [17–21]. The optimal power flow based on an iterative method have been modified to consider recently composed DC components as revealed in [22]. The study in [22] considers a voltage-sourced converter (VSC) based on high voltage DC in the power flow equation to improve accuracy and stability in power system analysis. Meanwhile, the pure DC network also utilized an iterative method in a nodal analysis [23]. The methods are normally formed to find the DC voltage level at each node in state analysis. These processes are influenced by the scale of the system matrix in terms of calculation time, which is a major problem in the order management plan of a real-time controller [24].

The aim of this paper is to present a feasibility study on the power flow analysis approach to improve accuracy of managing a hybrid system which consist of several DESs, incorporating the characteristics of main controller. Figure 1 illustrates the typical figure of the controller structure highlighting the target processes. A storage system is included in the structure connected to the main PCS with a boost chopper device. Together with the storage device, the PV modules are expected to connect to the main PCS as a hybrid form. Several current flows from DESs will form DC current (i_{dcn}) and be imposed on the main PCS and the measured signals (i_n) used in the highlighted section for voltage calculation.

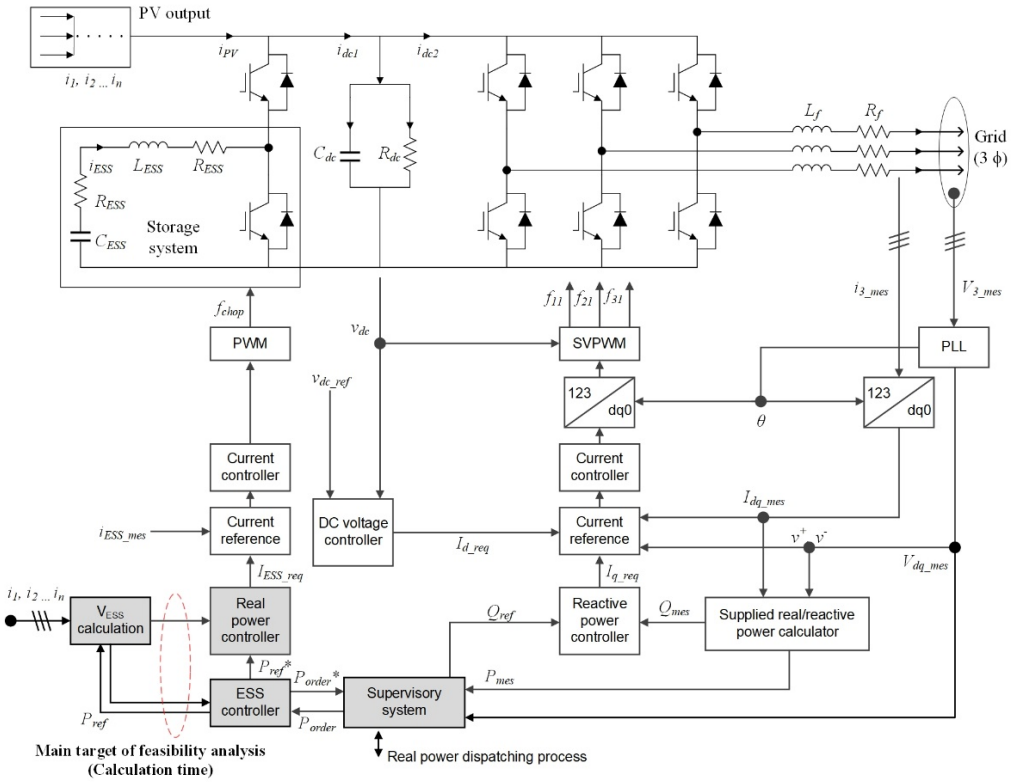

Figure 1. Typical structure of a photovoltaic (PV)-energy storage system (ESS) power conversion system. PLL, phasor locked loop.

A typical control flow for VSC is applied. The measured DC voltage (v_{dc}) is used in the PCS controller for grid-side, and the controller is independent of the real power control for connected DESs in the DC section. The determined reference for DC system operation (v_{dc_ref}) handles PCS signals based on measured values at grid side phasor locked loop (PLL). These control flows are for composing a PV generation system that could follow maximum power point tracking process. When a monitoring system receives a real power order from a TSO, a real power control for the entire DC system is operated independently. Without a signal correction scheme, the real power command for the ESS ignores a voltage variation in the DC section. However, based on a PV current flow signal, a modified value could be generated in this concept to decide the final reference signal for the power controller. The likely issues that may be encountered when the calculation process is applied to existing controls are illustrated in Figure 2. After constructing the line matrix for power flow analysis, a delay can be generated according to the size of the matrix for its complementation process. As the size of PV increases, the possibility of time delay is expected to increase since the calculation load for signal correction depends on the number of modules.

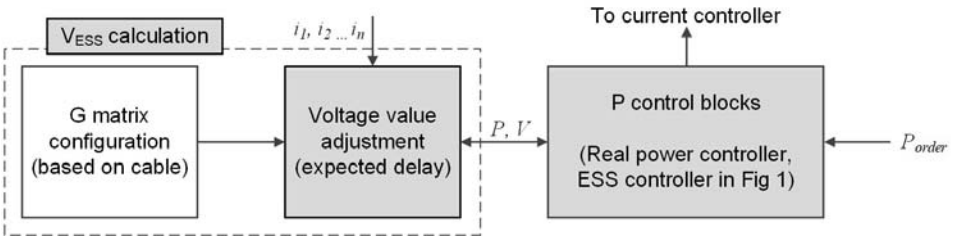

Figure 2. Description of added block for accuracy improvement method.

2.2. Hybrid System

The hybrid model used in this paper focuses on the structure of combined energy resources. It is expected that all the power generated by the DES passes through the main PCS. If an ESS is included, it must be able to comply with the TSO's order according to the current flow variation in the main PCS. Sectional losses and errors are frequent in coupled DC networks as described in [25] and approaches to these issues were being studied [26]. However, if a combined DC system expands its size, the low DC voltage may generate unstable conditions and require precise techniques to comply with imposed orders. In this study, the hybrid model was employed and a compensation technique that can reflect the voltage fluctuations of each DC section applied.

2.3. PV Plant Configuration

Typical information of a PV generation system is shown in Table 1. A PV system contains inverters by based on own topology: central, string, multistring, and module integrated. The general form of the hybrid system takes a large-scale PV farm that is suitable for the ESS compensation plan. Thus, central and multistring topologies (more than 30 kilowatts (kW)) would be appropriate in this analysis. The PV connection that includes the inverter and transformer based on both topologies is described in Figure 3. As shown in the figure, in the case of a multistring topology, a common DC area is formed at connection point of several single strings. Since the DC-DC converters could measure each connection point of the string, a power flow analysis for generating a modified ESS signal could be simplified. In other words, the feasibility study for the multistring topology can be progressed based on one single array that makes up a string (the matrix for the modules is larger than that of the converters). The generalized string structure in [27] is used in this analysis. To secure the robustness in terms of power extraction, a MW-scaled PV is connected to the grid through a central inverter topology [28]. With the topology, a mega-voltage-ampere (MVA) class DC/AC inverter can accommodate several thousands of PV panels. However, unlike other topologies, the central topology exhibits low levels of flexibility and high mismatching losses due to its huge configuration characteristics.

As mentioned earlier, the main focus of this paper is to check control constraint of the accuracy improvement plan. A more detailed description of the structure can be found in [13]. In order to explain the ESS operation plan, a DC power flow method applied on two topologies is described in Section 3. In addition, simulation studies to find availability according to expected delays are discussed in Section 4.

Table 1. Numerical information of PV inverter topologies.

Topology	P (kW)	V_{dc} Range (V)	V_{ac} Range (V)	f (Hz)
Central	100–1500	400–1000	270–400	50, 60
String	0.5–5	200–500	110–230	50, 60
Multistring	2–30	200–800	270–400	50, 60
Module integrated	0.06–0.5	20–100	110–230	50, 60

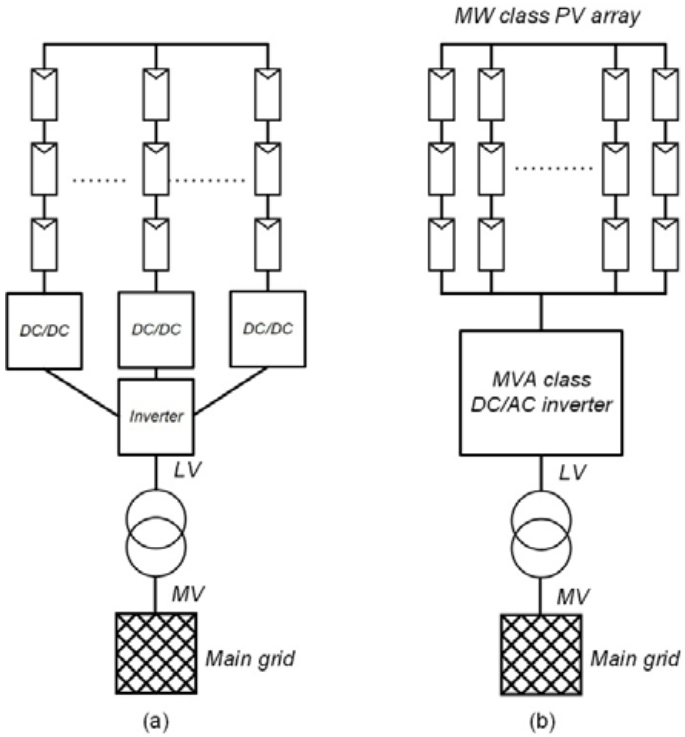

Figure 3. Configuration of PV inverter topologies (**a**) multistring (**b**) central.

3. DC Flow Analysis

To perform a current flow analysis of the defined DC network, an electricity-based circuit model is required. The nodal analysis method based on the presented PV circuit was used. In this method, an admittance matrix which includes cable components is adjusted in power flow analysis according to the PV power extraction.

For the general analysis of PV circuits for current estimation, the admittance of the components was divided into two categories (consumption and supply) for simplicity. With these simplifications, the PV current can then be reflected in the matrix representation. In a PV system, a current flows through the cathode for grounding. According to [13], a method was used to eliminate the current leakage in consideration of ground impedance. Since this study examined the impact of computational load with a focus on a previously used method of deriving current expectation based on real-time power output, the detailed resistance component between each PV module is applied to the admittance matrix. A consideration is made of the resistance component of the DC pole of the cathode which is generally considered as the ground section.

In this study, the nodal analysis was applied to formulate the detailed current flow in DC section. With this, the PV system can convert the energy extraction state of each module into a current flow. The output power of the PV module can be changed as a negative admittance component to be included in the matrix. In the case of an ESS, the charging and discharging power can be implemented as equivalent components according to the amount of profile. Based on a single module, each component can be represented by an admittance matrix as follows:

$$g = \begin{vmatrix} G_P & -G_{PN} & -G_{P0} & 0 \\ -G_{PN} & G_N & 0 & 0 \\ -G_{P0} & 0 & G_{PCS} & -G_{DC} \\ 0 & 0 & -G_{DC} & G_{ESS} \end{vmatrix} \quad (1)$$

The diagonals of the admittance matrix for positive/negative node of module and connection points of PCS, ESS (G_P, G_N, G_{PCS}, G_{ESS}) includes power extractions along with connected cable component as follows:

$$G_P = g_n + g_{Pnn-1} \tag{2}$$

$$G_N = g_n + g_{Nnn-1} \tag{3}$$

$$G_{PCS} = g_{Nnn-1} + g_{PCS} + g_{dc-dc} \tag{4}$$

$$G_{DC} = g_{dc-dc} + g_{ESS} \tag{5}$$

The non-diagonals of the admittance matrix for positive/negative section are solely composed with regarded cable (g_{Pnn-1}, g_{Nnn-1}) or equivalent admittance of own conversion system ($g_{dc\text{-}dc}$, g_{ESS}). When adding n modules, the size of the admittance matrix adds $n \times 2$ columns and rows on the basis of generalized matrix (1). Based on this, it is possible to analyze a mean conversion time for a large PV system and organize a feasibility study whether the expected delay is within a constraint.

In the iterative process, it is necessary to define an input variable with previous state (k) that can reflect the amount of output power to estimate the voltage level of the DC section which is considered as an unknown value. The corresponding input parameter must be converted to an admittance value, and the power extracted from each PV module connected in series can be updated repeatedly as follows:

$$g_{n\cdot k} = -\frac{P_{n\cdot k}}{(V_{Pn\cdot k} - V_{Nn\cdot k})^2} \tag{6}$$

The admittance component for ESS is able to be expressed as shown in Equation (7) considering grounding.

$$g_{ESS\cdot k} = -\frac{P_{ESS\cdot k}}{V_{ESS\cdot k}^2} \tag{7}$$

The voltage in each section for next state (k + 1) is affected by the admittance factor due to the modified value until it converges within the available range. The main PCS current is fixed for convergence as a slack element. To perform the iterations considered as the main calculation, the inverse matrix is used to advance the iteration method as described in (8). The generalized control diagram is illustrated in Figure 4.

$$[V_{k+1}] = [g_k]^{-1} \times [I_k] \tag{8}$$

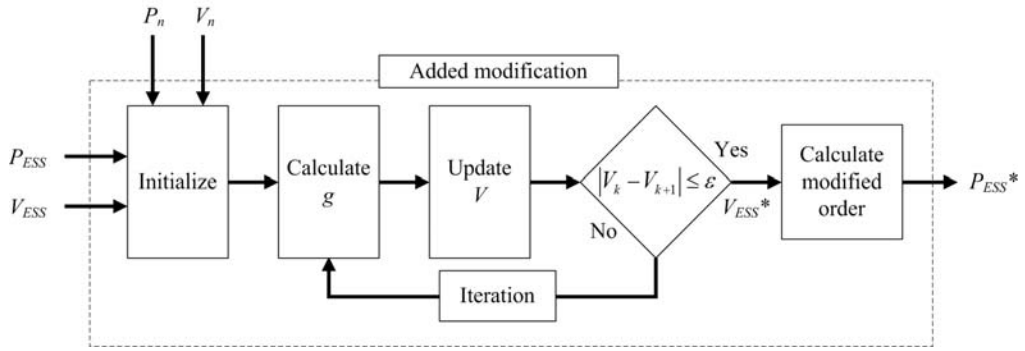

Figure 4. Modified control diagram of iterative method.

The contents of (1) depends on the number of PV modules, hence, a large-scale PV generation system requires further dimensional matrix. If n modules are added, the circuit will be expanded as mentioned earlier which results in a change of the basic equation as given in (9). Based on the

configured sparse matrix, an analysis of the possible computational load and delay effect on main controller was performed using case studies.

$$\begin{vmatrix} g_1+g_{P1n} & -g_1 & \cdots & -g_{P1n} & 0 & \cdots & 0 & 0 \\ -g_1 & g_1+g_{N1n} & \cdots & 0 & -g_{N1n} & \cdots & 0 & 0 \\ \vdots & \vdots & \ddots & \vdots & \vdots & \iddots & \vdots & \vdots \\ -g_{P1n} & 0 & \cdots & g_{P1n}+g_n+g_{Pn0} & -g_n & \cdots & -g_{Pn0} & 0 \\ 0 & -g_{N1n} & \cdots & -g_n & g_{N1n}+g_n+g_{Nn0} & \cdots & 0 & 0 \\ \vdots & \vdots & \iddots & \vdots & \vdots & \ddots & \vdots & \vdots \\ 0 & 0 & \cdots & -g_{Pn0} & 0 & \cdots & g_{Pn0}+g_{PCS}+g_{dc-dc} & -g_{dc-dc} \\ 0 & 0 & \cdots & 0 & 0 & \cdots & -g_{dc-dc} & g_{dc-dc}+g_{ESS} \end{vmatrix} \begin{vmatrix} V_{u1} \\ V_{d1} \\ \vdots \\ V_{dn} \\ V_{dn} \\ \vdots \\ V_{dc} \\ V_{ESS} \end{vmatrix} = \begin{vmatrix} 0 \\ 0 \\ \vdots \\ 0 \\ 0 \\ \vdots \\ i_{dc} \\ 0 \end{vmatrix} \quad (9)$$

4. Simulation

4.1. Simulation Design

To verify the effectiveness of the control method, a simulation was performed using PSCAD (power system computer-aided design). Figure 5 shows a design of the network with PV sources configuring a common DC section that includes ESS. The basic rated power capacity of a single PV is 400 kVA. The designed PV system was connected to a displayed distribution network through an inverter topology (multistring and central). Preferentially, the individual unit of a PV system is composed of a single string to check calculation load of the multistring scheme (three strings are used for PV). Next, an expanded feasibility test was then carried out with an integrated 1.2 MW PV system with consideration of the maximum computational load as well. The distance of the pi line was reflected using generic model in PSCAD (library with *R*, *Xl*, *Xc* elements), and the residual information is given in Table 2.

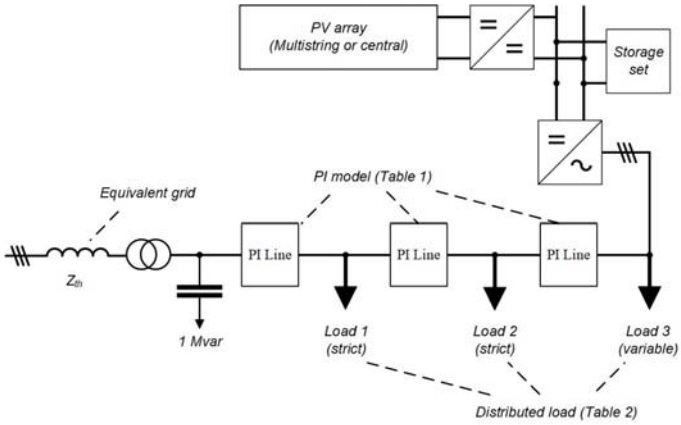

Figure 5. Simulated distribution network including MW scale PV/ESS.

The configured PV system extracts real power based on environmental variables, as in the previous study. DC voltage fluctuations due to the extracted power may affect the operation of the connected ESS. To continue the feasibility studies based on the verified charging/discharging pattern of ESS, load fluctuations (Figure 6) and ESS control effects (Figure 7) were used. The AC grid voltages at each load connection site are described in Figure 8 to confirm if it causes an impact on the DC network in the simulation. The RMS magnitudes are classified according to the distance from the substation and each section is maintained with stable conditions. The main objective of the simulation is to confirm the reliability of the proposed method. For this reason, individual load fluctuations were designed and ESS operating signal configured to change according to load conditions. An analysis focusing the ESS control according to each load change proceeded.

Table 2. Numerical data for the simulation.

Specific Data	Value	Unit
Rated AC voltage	22.9	kV
Rated DC voltage	500	V
Distance between each module	0.5	Meter
Amount of load	3	
Rated energy of ESS	200	kWh
Rated power of ESS	200	kW
Rated power of PV system (one unit)	400	kW
PI (π) line distance	500	Meter
Substation voltage (HV)	154	kV
Substation MVA	60	MVA
Short-circuit ratio of utility grid	15	
X/R ratio of utility grid	15	

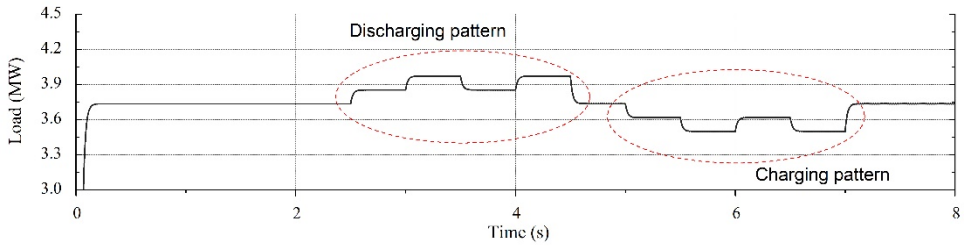

Figure 6. Imposed load variating condition for case study.

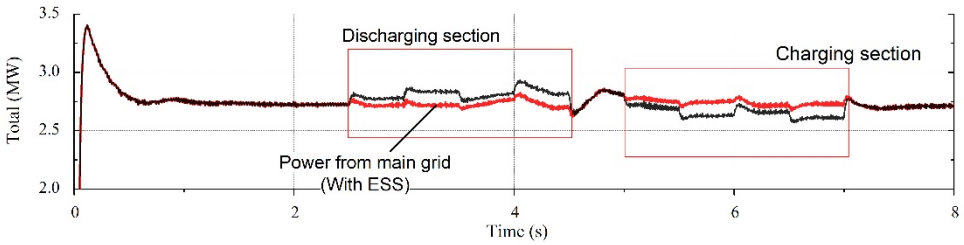

Figure 7. Power supply quantity from main grid in designed scenario (with and without ESS).

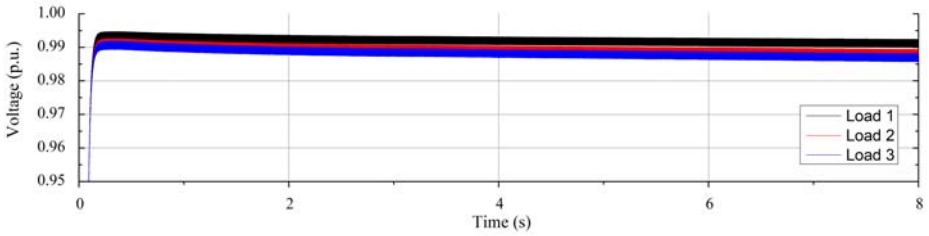

Figure 8. AC side root mean square (RMS) voltage at connection point for loads.

Table 3 details the load parameters applied to the case study. The total simulation time was defined in 8 seconds including initialization. Load changes were made in stages as shown in Figure 6. The ESS was configured to charging/discharging in response to an instantaneous load change (75 kW). The derived average iteration number (adjusting the input values) and expected average solution time, for each topology were represented together. Taking into account the configuration that a single string has 40 modules, the multistring topology configured a system matrix. In the case of the central topology, it was designed with three parallel units that were used for a single string. The number of iterations were not change in each topology, however, the expected solution time increased and the regarded delay increased as well. In this paper, the plan was to apply the 100 ms (10 Hz calculation frequency) interval to the multistring topology and apply not only 200 ms (5 Hz) to the central topology,

but 400 ms (2.5 Hz) to consider the additional computational load. If the calculation is not terminated within the imposed constraint, the previous value must be used until the calculation is completed.

Table 3. Simulated case study description.

Simulation Time	8 Seconds (s)
Base load condition (Real power)	Load 1: 900 kW, Load 2: 1,500 kW, Load 3: 1,380 kW
Load increase sections (Load 3)	2.5–3, 3.5–4 s (75 kW) 3–3.5, 4–4.5 s (150 kW)
Load decrease sections (Load 3)	5–5.5, 6–6.5 s (75 kW) 5.5–6, 6.5–7 s (150 kW)
Iterations	3 (multistring), 3 (central)
Required solution time	95 millisecond (ms), (multistring) 185 ms (central)
Imposed maximum interval of calculation	100 ms (multistring) 200, 400 ms (central)

Within the improvement effect shown in Figure 7, the simulation was configured to deduce availability by showing how computational delay affects control. One of the objectives of this study was to confirm if the utilized control can reduce the possible error compared to the strict voltage control as well perform an adequate power supply with expected delay.

4.2. Simulation Results

An availability study should ensure that voltage corrections can be managed with limited calculation capability. The analysis of the charging and discharging sections (2.5–4.5 and 5–7 seconds), which were the main focus of this analysis are explained sequentially. Figure 9 shows the delay effect that can be derived from the multistring topology compared to the pre-analyzed method (strict-voltage, voltage-estimation). It can be confirmed that both charging and discharging are not significantly affected by the delay. The output control was observed to be performed substantially in the same manner as the accuracy improvement method without any delay. In the multistring topology, it was confirmed that the control signal can be derived within the maximum calculation load. Figure 10; Figure 11 show the delay effects that can be derived from the central topology. It can be confirmed that the influence of the delay occurs in both places, however, the control proceeds within a range that did not reach the strict-voltage method. In the case of Figure 11, including the maximum calculation load, an error occurs with a high probability, but it was confirmed that the occurrence of the delay was not frequent.

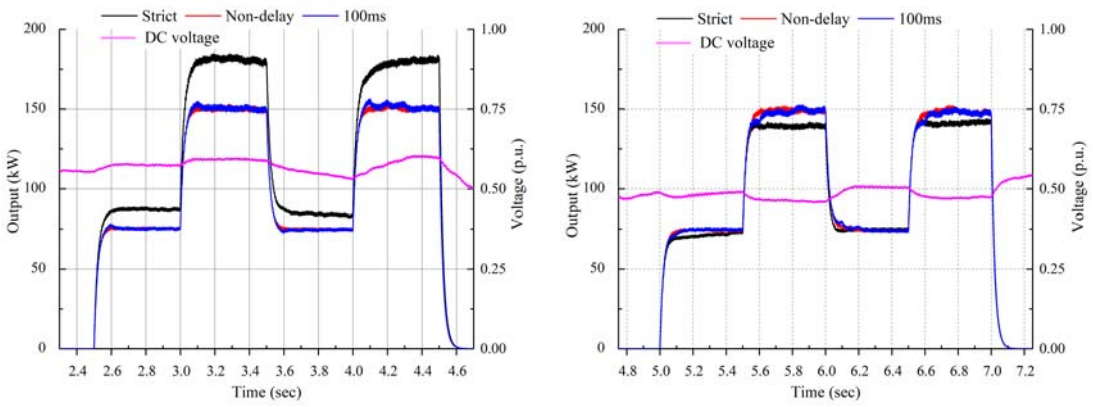

Figure 9. ESS states for multistring topology with 100 ms interval (**a**) extracted power quantity in the discharging section (2.5 to 4.5 s); (**b**) absorbed power quantity in the charging section (5 to 7 s).

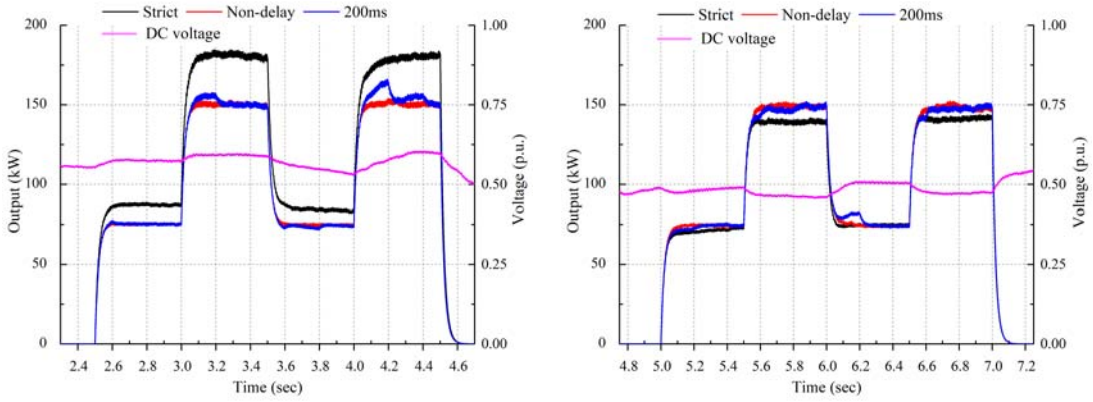

Figure 10. ESS states for central topology with 200 ms interval (**a**) extracted power quantity in the discharging section (2.5 to 4.5 s); (**b**) absorbed power quantity in the charging section (5 to 7 s).

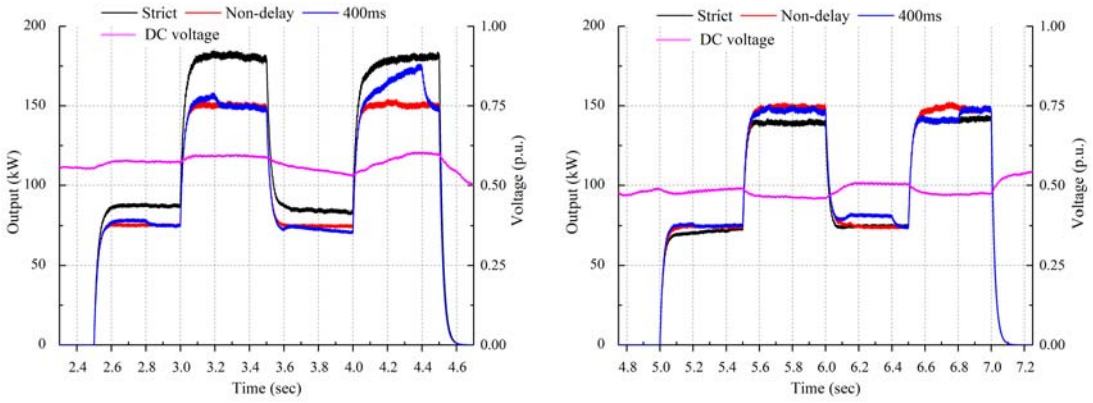

Figure 11. ESS states for central topology with 400 ms interval (**a**) extracted power quantity in the discharging section (2.5 to 4.5 s); (**b**) absorbed power quantity in the charging section (5 to 7 s).

Table 4 shows the errors in terms of power support for designed scenarios. Compared to the ideal case (voltage-estimation without delay), the multistring topology could lose minor accuracy in terms of power support, and the central topology with 5 Hz calculation frequency shows less than 5 percent mismatch. It seems that a large mismatch can be induced with the central topology when considers maximum calculation load, however, it is expected to be generated on the oversized PV scale. The utilized signal correction scheme seems to be available with a normalized PV system in consideration of the possible delay ranges.

Table 4. Comparison data for designed simulation.

Imposed Constraint	ESS Mode	Demanded Quantity (Wh)	Accomplished Quantity (Wh)	Supply Accuracy (%)
Non-delay	Charging	125	121.212	96.97
	Discharging	125	123.731	98.98
10 Hz	Charging	125	121.101	96.88
	Discharging	125	123.911	98.98
5 Hz	Charging	125	119.303	95.34
	Discharging	125	126.282	98.97 (exceed)
2.5 Hz	Charging	125	117.92	94.33
	Discharging	125	134.9	92.08 (exceed)

5. Conclusions

This paper confirms the feasibility of the voltage-estimation method for a MW-scaled hybrid system. Existing signal correction methods to assist ESS operation were analyzed and utilized. The possible delays in calculations that occur with real power management were used in case studies. In designed simulation, the voltage-estimation method showed robustness in target topologies (multistring, central).

In response to the changed load condition, the voltage-estimation method acts to generate a modified order considering the actual required power extraction and calculation load. Focusing on the computational load caused by the expansion of a single PV system, we have analyzed the convergence of the PCS signal with the iteration method. With respect to this, a calculation delay could be generated not only by the PV module, but also by the applied sensor. Although this can be improved with detailed gain adjustments or by using a correction method according to the response characteristics, these circumstances need to be considered in the ESS management plan in advance. Therefore, a possible situation about signal calculation was derived, tested, and listed based on previous simulation design. In the aspect of the inverter topology, the possible delays need to be considered in advance when configuring the system. This operation can improve the accuracy both of the state of charge estimation and response operation.

Author Contributions: Conceptualization, J.S. and S.J.; Methodology, S.J.; Software, J.S.; Validation, J.S., and S.J.; Formal analysis, J.S., S.J.; Investigation, M.Y.; Data curation, M.Y.; Writing—original draft preparation, S.J.; Writing—review and editing, J.S. and S.J.; Supervision, S.J.; Project administration, S.J.; Funding acquisition, S.J. All authors have read and agreed to the published version of the manuscript.

Funding: This work was supported by the National Research Foundation Grant (No. 2018R1C1B5030524) and the Korea Electric Power Corporation Grant (R18XA06-40) funded by the Korean government.

Conflicts of Interest: The authors declare no conflict of interest.

Nomenclature

g_n	Equivalent admittance of nth module
g_{Pnn-1}	Admittance of positive side DC cable between modules
g_{Nnm-1}	Admittance of negative side DC cable between module
g_{dc-dc}	Equivalent admittance about DC/DC convertor for ESS
g_{ESS}	Equivalent admittance of ESS module
P_n	Injected power wt nth node
V_{Pn}	Upper-side voltage of nth module
V_{Nn}	Lower-side voltage of nth module
V_{dc}	Collector voltage
V_{ESS}	Induced ESS voltage
k	Iteration number

References

1. Rakhshani, E.; Rouzbehi, K.; J. Sánchez, A.; Tobar, A.C.; Pouresmaeil, E. Integration of Large Scale Pv-Based Generation into Power Systems: A Survey. *Energies* **2019**, *12*, 1425. [CrossRef]
2. Jo, B.-K.; Jung, S.; Jang, G. Feasibility Analysis of Behind-The-Meter Energy Storage System According to Public Policy on an Electricity Charge Discount Program. *Sustainability* **2019**, *11*, 186. [CrossRef]
3. IEEE Standard for Interconnection and Interoperability of Distributed Energy Resources with Associated Electric Power Systems Interfaces. In *IEEE Std 1547-2018 (Revision of IEEE Std 1547-2003)*; IEEE: Piscataway, NJ, USA, 2018.
4. Osório, G.J.; Shafie-khah, M.; Lujano-Rojas, J.M.; Catalão, J.P. Scheduling Model for Renewable Energy Sources Integration in an Insular Power System. *Energies* **2018**, *11*, 144. [CrossRef]
5. Subramani, G.; Ramachandaramurthy, V.K.; Padmanaban, S.; Mihet-Popa, L.; Blaabjerg, F.; Guerrero, J.M. Grid-tied Photovoltaic and Battery Storage Systems with Malaysian electricity tariff—A review on maximum demand shaving. *Energies* **2017**, *10*, 1884. [CrossRef]

6. Zeng, Z.; Yang, H.; Zhao, R.; Cheng, C. Topologies and Control Strategies of Multi-Functional Grid-Connected Inverters for Power Quality Enhancement: A Comprehensive Review. *Renew. Sustain. Energy Rev.* **2013**, *24*, 223–270. [CrossRef]
7. Miao, L.; Wen, J.; Xie, H.; Yue, C.; Lee, W. Coordinated Control Strategy of Wind Turbine Generator and Energy Storage Equipment for Frequency Support. *IEEE Trans. Ind. Appl.* **2015**, *51*, 2732–2742. [CrossRef]
8. Bird, L.; Cochran, J.; Wang, X. *Wind and Solar Energy Curtailment: Experience and Practices in the United States*; NREL: Golden, CO, USA, 2014.
9. Chen, P.; Thiringer, T. Analysis of Energy Curtailment and Capacity Over installation to Maximize Wind Turbine Profit Considering Electricity Price - Wind Correlation. *IEEE Trans. Sustain. Energy* **2017**, *8*, 1406–1414. [CrossRef]
10. Saez-de-Ibarra, A.; Milo, A.; Gaztañaga, H.; Debusschere, V.; Bacha, S. Co-Optimization of Storage System Sizing and Control Strategy for Intelligent Photovoltaic Power Plants Market Integration. *IEEE Trans. Sustain. Energy* **2016**, *7*, 1749–1761. [CrossRef]
11. Stimoniaris, D.; Tsiamitros, D.; Dialynas, E. Improved Energy Storage Management and PV-Active Power Control Infrastructure and Strategies for Microgrids. *IEEE Trans. Power Syst.* **2016**, *31*, 813–820. [CrossRef]
12. Vargas, L.S.; Bustos-Turu, G.; Larraín, F. Wind Power Curtailment and Energy Storage in Transmission Congestion Management Considering Power Plants Ramp Rates. *IEEE Trans. Power Syst.* **2015**, *30*, 2498–2506. [CrossRef]
13. Yoo, Y.; Jang, G.; Kim, J.-H.; Nam, I.; Yoon, M.; Jung, S. Accuracy Improvement Method of Energy Storage Utilization with DC Voltage Estimation in Large-Scale Photovoltaic Power Plants. *Energies* **2019**, *12*, 3907. [CrossRef]
14. Zhang, H.; Yue, D.; Xie, X. Robust Optimization for Dynamic Economic Dispatch Under Wind Power Uncertainty with Different Levels of Uncertainty Budget. *IEEE Access* **2016**, *4*, 7633–7644. [CrossRef]
15. Byungdoo, J.; Hyun, K.; Heechan, K.; Hansang, L. Development of a Novel Charging Algorithm for On-board ESS in DC Train through Weight Modification. *J. Electr. Eng. Technol.* **2014**, *9*, 1795–1804.
16. Padrlőn, J.F.M.; Lorenzo, A.E.F. Calculating Steady-State Operating Conditions for Doubly-Fed Induction Generator Wind Turbines. *IEEE Trans. Power Syst.* **2010**, *25*, 922–928.
17. Li, S. Power Flow Modeling to Doubly-fed Induction Generators (DFIGs) Under Power Regulation. *IEEE Trans. Power Syst.* **2013**, *28*, 3292–3301. [CrossRef]
18. Yu, H.; Rosehart, W.D. An Optimal Power Flow Algorithm to Achieve Robust Operation Considering Load and Renewable Generation Uncertainties. *IEEE Trans. Power Syst.* **2012**, *27*, 1808–1817. [CrossRef]
19. Liu, S.; Xu, Z.; Hua, W.; Tang, G.; Xue, Y. Electromechanical Transient Modeling of Modular Multilevel Converter Based Multi-Terminal HVDC Systems. *IEEE Trans. Power Syst.* **2014**, *29*, 72–83. [CrossRef]
20. Sun, H.; Guo, Q.; Zhang, B.; Guo, Y.; Li, Z.; Wang, J. Master-slave-splitting Based Distributed Global Power Flow Method for Integrated Transmission and Distribution Analysis. *IEEE Trans. Smart Grid.* **2015**, *6*, 1484–1492. [CrossRef]
21. Mumtaz, F.; Syed, M.H.; Hosani, M.A.; Zeineldin, H.H. A Novel Approach to Solve Power Flow for Islanded Microgrids Using Modified Newton Raphson with Droop Control of DG. *IEEE Trans. Sustain. Energy* **2016**, *7*, 493–503. [CrossRef]
22. Yang, Z.; Zhong, H.; Bose, A.; Xia, Q.; Kang, C. Optimal Power Flow in AC–DC Grids with Discrete Control Devices. *IEEE Trans. Power Syst.* **2018**, *33*, 1461–1472. [CrossRef]
23. Cai, Y.; Irving, M.R.; Case, S.H. Iterative Techniques for the Solution of Complex DC-rail-traction Systems including Regenerative Braking. *IEE Proc. Gener. Transm. Distrib.* **1995**, *142*, 445–452. [CrossRef]
24. Pyzara, A.; Bylina, B.; Bylina, J. The Influence of a Matrix Condition Number on Iterative Methods' Convergence. In Proceedings of the 2011 Federated Conference on Computer Science and Information Systems (FedCSIS), Szczecin, Poland, 18–21 September 2011; pp. 459–464.
25. Karthikeyan, V.; Gupta, R. Multiple-Input Configuration of Isolated Bidirectional DC–DC Converter for Power Flow Control in Combinational Battery Storage. *IEEE Trans. Ind. Informat.* **2018**, *14*, 2–11. [CrossRef]
26. Chew, B.S.H.; Xu, Y.; Wu, Q. Voltage Balancing for Bipolar DC Distribution Grids: A Power Flow Based Binary Integer Multi-Objective Optimization Approach. *IEEE Trans. Power Syst.* **2019**, *34*, 28–39. [CrossRef]

27. Planning of a PV Generator 2013, SMA Solar Technology AG. Available online: https://files.sma.de/dl/1354/DC-PL-en-11.pdf (accessed on 1 December 2019).
28. Cabrera-Tobar, A.; Bullich-Massagué, E.; Aragüés-Peñalba, M.; Gomis-Bellmunt, O. Topologies for Large Scale Photovoltaic Power Plants. *Renew. Sustain. Energy Rev.* **2016**, *59*, 309–319. [CrossRef]